

Transformation Relations for *UBV* Photometric System of 1m Telescope at the TÜBİTAK National Observatory

T. Ak^{1*} , R. Canbay² , and T. Yontan¹ 

¹Istanbul University, Faculty of Science, Department of Astronomy and Space Sciences, 34119, İstanbul, Türkiye

²Istanbul University, Institute of Graduate Studies in Science, Programme of Astronomy and Space Sciences, 34116, İstanbul, Türkiye

ABSTRACT

UBV CCD observations of standard stars selected from Landolt (2009, 2013) were performed using the 1-meter telescope (T100) of the TÜBİTAK National Observatory equipped with a CCD camera and Bessell *UBV* filters. Observations were conducted over an extended period, spanning from 2012 to 2024, covering a total of 50 photometric nights. Photometric measurements were used to find the standard transformation relations of the T100 photometric system. The atmospheric extinction coefficients, zero points and transformation coefficients of each night were determined. It was observed that the primary extinction coefficients decreased until the year 2019 and increased after that year. Strong seasonal variations in the extinction coefficients were not evident. Small differences in seasonal median values of them were used to attempt to find the atmospheric extinction sources. We found calculated minus catalogue values for each standard star, $\Delta(U-B)$, $\Delta(B-V)$, and ΔV . The means and standard deviations of these differences were estimated to be 1.4 ± 76 , 1.9 ± 18 , and 0.0 ± 36 mmag, respectively. We found that our data well matched Landolt's standards for *V* and *B-V*, i.e. there are no systematic differences. However, there are systematic differences for *U-B* between the two photometric systems, which is probably originated from the quantum efficiency differences of the detectors used in the photometric systems, although the median differences are relatively small ($|\Delta(U-B)| < 50$ mmag) for stars with $-0.5 < (U-B) < 1.6$ and $0.2 < (B-V) < 1.8$. We conclude that the transformation relations found in this study can be used for standardised photometry with the T100 photometric system.

Keywords: Techniques: CCD photometry; stars: imaging; standard star

1. INTRODUCTION

The instrumental magnitude of a celestial object measured during an astronomical observation depends not only on the object's flux and atmospheric extinction but also on the spectral response and transmission properties of the telescope-filter-detector combination. In some cases, instrumental magnitudes must be transformed into a standard photometric system by observing standard stars. The 'Johnson-Kron-Cousins' *UBVR_CI_C* system is the most widely used broad-band photometric system. The *UBV(RI)* photometric system was designed by Johnson & Morgan (1953) taking Yerkes Atlas system (MK) of spectral classification as standard. In this photometric system, the colour indices of the bright star Vega with spectral type A0 was defined as the zero point of all colour indices. Due to advancements in detector technologies, accurate photometry of faint stars became possible in the 1970s and 1990s, and the Kron-Cousins *R_CI_C* filters were replaced with *RI* filters of Johnson and Morgan.

There are two main sets of standard stars used for broad-

magnitudes are generally linear as combined spectral responses of filter and detector are very similar (see, Sung & Bessell 2000).

Detailed information of photometric observing systems, including atmospheric extinction coefficients and transformation relations, is crucial for standardized photometry. In a series of *UBV* photometric observations of open stellar clusters between the years 2012 and 2024, we have also observed Landolt's selected standard star fields for each observing night with Bessell *UBV* filters attached to an SI 1100S CCD camera and 1-meter telescope of the TÜBİTAK National Observatory. Atmospheric extinction coefficients and transformation equations to standard photometric systems were calculated for each photometric night. Although the observations have not been done specifically for monitoring the extinction and transformation coefficients of this photometric system, we could obtain them as a side-product of our observations. In this study, we investigate the variation of atmospheric extinction coefficients for the last 12 years and introduce a reliable set of *UBV* transformation relations for the photometric observing system of the 1-meter telescope (T100) at the TÜBİTAK National Observatory.

Corresponding Author: T. Ak E-mail: tanselak@istanbul.edu.tr

Submitted: 25.10.2024 • **Accepted:** 04.12.2024



This article is licensed under a Creative Commons Attribution-NonCommercial 4.0 International License (CC BY-NC 4.0)

2. OBSERVATIONS AND DATA REDUCTION

All the observations have been performed with the 1-meter telescope (T100) of TÜBİTAK National Observatory. The T100 telescope has a Ritchey-Chretien optical system with an $f/10$ focal ratio which provides a wide field of view using appropriate 3-element field lenses¹. T100 is equipped with an SI 1100 CCD camera and Bessell UBV filters. Specifications of the camera are given in Table 1¹. The camera has a Fairchild 486 Back Illuminated and UV-enhanced chip, which covers a field of view of $21'.5 \times 21'.5$. Quantum efficiency (QE) of the chip is shown in Figure 1². QE of the chip across the U passband is very good, i.e. its QE is $\sim 65\%$ at $\lambda=300$ nm and $\sim 92\%$ at $\lambda=400$ nm. Transmittance curves of the Bessell UBV filters are presented in Figure 2³. Note that the B filter has a very weak visual leak centered at ~ 560.5 nm with a maximum transmittance of $\sim 1.6\%$. Since the transmittance of Bessell U filter starts at ~ 315 nm and peaks at ~ 370 nm, QE curve of the chip covers this filter with acceptable sensitivity. QE of the chip is also high for the Bessell B and V filters. It should also be noted that all the observations were done with the 2×2 binning mode of the camera to save the data downloading time and observe fainter stars with a high S/N ratio.

Stellar fields including standard stars selected from Landolt (2009, 2013) have been observed with Bessell UBV filters during 50 nights from 18 July 2012 to 29 September 2024. The fields with red and blue standards were preferred to find the colour dependence of atmospheric extinction. Each field was observed at least three times using Bessell UBV filters at the same airmass in order to estimate averages of stellar magnitudes. Image Reduction and Analysis Facility (IRAF⁴) routines were utilized for pre-reduction processes, bias subtraction and flat fielding the images. We did not perform dark frame subtraction since the camera's dark level is negligible. The instrumental magnitudes of the standard stars were measured utilizing IRAF software packages with aperture photometry.

3. RESULTS

3.1. Extinction coefficients and zero points

Atmospheric extinction is caused primarily by Rayleigh scattering and absorption from gas molecules, dust particles and aerosols in the atmosphere. The amount of extinction depends primarily on airmass but also varies with wavelength and color. These extinction dependencies are corrected by using a primary (or first) extinction coefficient, which depends on airmass, and a secondary extinction coefficient which depends also on colour. In addition, transformation coefficients are needed to transform the extra-atmospheric magnitudes to the standard photometric

Table 1. Specifications of the SI 1100S camera attached to the T100 telescope of TÜBİTAK National Observatory.

Camera	Spectral Instruments 1100S Cryo, UV, AR, BI
Chip	Fairchild 486 Back Illuminated
Read-out channels	4 channels
Pixel Number	4096×4037
Pixel Size	15×15 micron
Chip Size	61.44×61.44 mm
Gain	$0.57 e^-/ADU$ (@ 100 kHz)
Noise	$4.11 e^-$ (@ 100 kHz)
Bias level	~ 500 ADU
Dark Current	$0.0001 e^-/\text{pixel}/\text{sec}$
Well Depth	$142900 e^-$
Dynamic Range	16 bit
Chip Size	61.44×61.44 mm
Shutter	Bonn 80, Slit Type
Exposure Range	1 msec to 3600 sec
Cooling Method	Cryo-tiger
Operating Temp.	-100°C
PC Interface	Gigabit F/O kart (PCI)
Transfer Time	48 sec (1×1 binning), 13 sec (2×2 binning)
Pixel Scale	$0''.31 \text{ pixel}^{-1}$
Field of View	$21'.5 \times 21'.5$
Software	Maxim DL 5.12
Filter Wheel	2 wheels with 8 holes (76×76 mm each)
Filters	Asahi Conventional Bessell $UBVR_C I_C$

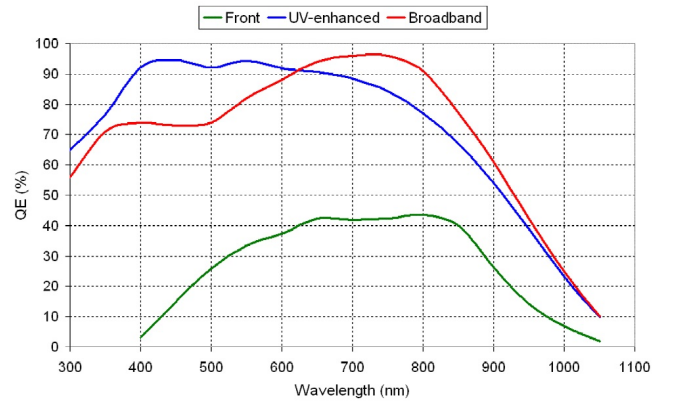


Figure 1. Quantum efficiency (QE) of the Fairchild 486 Back Illuminated chip attached to SI 1100S CCD camera. The UV-enhanced version (solid blue line) of the chip is used in our observations.

system. For V , $B - V$, and $U - B$, we derived coefficients of the form were given by Janes et al. (2013)

$$v = V + \alpha_{bv}(B - V) + k_v X + C_{bv}$$

$$b = V + \alpha_b(B - V) + k_b X + k'_b X(B - V) + C_b$$

$$u = V + (B - V) + \alpha_{ub}(U - B) + k_u X + k'_u X(U - B) + C_{ub}$$

where U , B , and V are the magnitudes in the standard photometric system. Parameters u , b , and v denote the instrumental magnitudes. X is the airmass. Parameters k and k' represent primary and secondary extinction coefficients. α and C are

¹ <https://tug.tubitak.gov.tr/en>

² <http://linmax.sao.arizona.edu/FLWO/48/CCD486DataSheetRevB.pdf>

³ <https://www.asahi-spectra.com/>

⁴ IRAF is distributed by the National Optical Astronomy Observatories

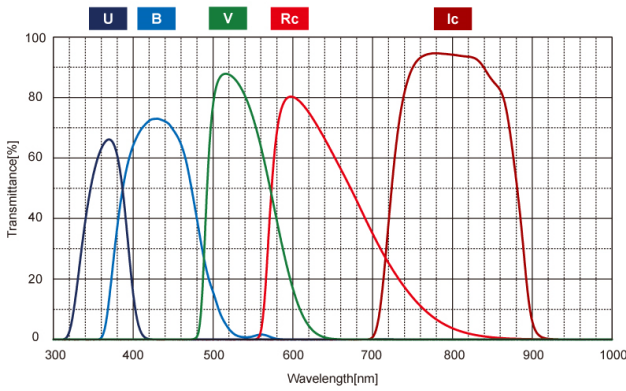


Figure 2. Transmittance curves of the conventional Bessell *UBV* filters of Asahi.

transformation coefficients to the standard photometric system and zero points, respectively. Multiple linear regression fits were applied to the transformation equations given above to estimate the photometric extinction and transformation coefficients with zero points for the observing nights. We determined atmospheric extinction and transformation coefficients under photometric conditions. Since we observed a considerable number of standard stars at different airmasses, we could obtain precise coefficients. The number of usable data points, the atmospheric extinction coefficients and zero points are given in Table 2.

The extinction coefficients in Table 2 span a 12-year observing period, although no observations were conducted in 2015 and 2017. The extinction coefficients in Table 2 cover a 12-year observing time, although no observations were conducted in 2015 and 2017. Median values of k_u , k_b , and k_v were calculated as 0.481 ± 0.097 , 0.303 ± 0.086 , and 0.174 ± 0.050 , respectively. Median secondary extinction coefficients k'_u and k'_b were found to be -0.048 ± 0.164 and -0.034 ± 0.072 . Error-values are standard deviations of the coefficients. Primary and secondary extinction coefficients can vary during the years depending on the atmospheric conditions of the observatory. Figure 3 exhibits such a slight variation of k_u , k_b , and k_v , where the increase after the year 2019 is prominent for *V* and *B* bands. These increases in extinction coefficients suggest that the photometric conditions at the observatory have gradually deteriorated since 2019. We could not detect considerable systematic increase or decrease in secondary extinction coefficients k'_u and k'_b .

Seasonal variations in primary extinction coefficients can help select appropriate observing nights for research projects. Unfortunately, it is not possible to find reliable median values of extinction coefficients obtained between December and February, since we have standard star observations for only two nights in this interval during the observing period of 12 years. Mean values of extinction coefficients of these two winter nights are $k_u=0.432 \pm 0.031$, $k_b=0.255 \pm 0.031$, and $k_v=0.149 \pm 0.009$, where errors are mean values of individual errors. Similarly,

we could observe standard stars only one night between March and May during 12 years of observing period. The remaining observations were performed summer (June-August) and autumn (September-November) seasons. Median values of extinction coefficients are $k_u=0.477 \pm 0.089$, $k_b=0.322 \pm 0.077$, and $k_v=0.191 \pm 0.051$ for summer season, while $k_u=0.502 \pm 0.113$, $k_b=0.279 \pm 0.098$, and $k_v=0.157 \pm 0.047$ for autumn season. There appears to be no significant seasonal difference in extinction coefficients between summer and autumn, as their median values are very similar within the margins of error. Based on the seasonal extinction coefficients and the number of usable nights, it is evident that winter and spring are not favorable seasons for photometric observations at the TÜBİTAK National Observatory.

It is known that instrumental parameters and atmospheric conditions affect the photometric zero point. The value of the photometric zero point depends on the size and condition (primarily mirror reflectivity) of the telescope and the quantum efficiency of the detector. Atmospheric conditions, such as water vapour content and height of the ozone layer, also affect the photometric zero points. The photometric zero points C_b , C_{bv} and C_{ub} measured during our observations are listed in Table 2. Variations of zero points are shown in Figure 4. As can be seen in Figure 4, variation of the zero points with time clearly exhibits the condition of the telescopic reflectivity. Beginning with the year 2012, reflectivity decreases (zero points become fainter) with time. Cleaning of the main mirror in August 2022 can be seen in Figure 4 as a sudden brightening of zero points.

3.2. Transformation coefficients

Transformation coefficients found from the standard star observations made during 50 nights between the years 2012 and 2024 are given in Table 3. Median values of the transformation coefficients are $\alpha_b=0.958 \pm 0.100$, $\alpha_{bv}=0.070 \pm 0.013$, and $\alpha_{ub}=0.886 \pm 0.228$, where errors are standard deviations of the individual values. We calculated possible maximum values by adding standard deviations to the median transformation coefficients. Using these maximum values, the resulting magnitudes differ by at most 25-30 mmag for a red star ($B - V = 1.9$ mag) compared to those calculated with median coefficients, assuming extinction coefficients and zero points remain constant.

3.3. Sources of extinction

Small seasonal differences in median extinction coefficients may result from extinction sources in the atmosphere. Atmospheric extinction is mainly a result of scattered light from molecules and small particles. The scattering efficiency depends on wavelength. The relation between the atmospheric extinction coefficients and wavelength can be expressed as $k_\lambda = \beta/\lambda^n$, where k_λ , β and λ are the extinction coefficient, an appropriate constant and the mean wavelength of filter (Golay 1974). If extinction is due to the Rayleigh scattering, then $n=4$.

Table 2. The atmospheric extinction coefficients and zero points obtained each observing night. Numbers in parentheses denote the number of usable data points. Median values are given in the last line, where errors are standard deviations of the individual values.

Date	k_u	k_b	k_v	$k_{u'}$	$k_{b'}$	C_b	C_{bv}	C_{ub}
2012.07.18	0.597±0.032(38)	0.392±0.022(52)	0.247±0.005(52)	-0.058±0.032	-0.030±0.019	0.771±0.050	0.799±0.010	3.111±0.054
2012.07.19	0.472±0.031(82)	0.326±0.024(85)	0.189±0.024(85)	-0.019±0.032	-0.057±0.025	0.745±0.036	0.799±0.017	3.143±0.046
2012.07.20	0.559±0.033(39)	0.392±0.011(30)	0.235±0.002(41)	-0.002±0.035	-0.037±0.011	0.786±0.017	0.838±0.005	3.190±0.054
2012.08.16	0.677±0.030(63)	0.525±0.050(58)	0.242±0.007(73)	-0.023±0.067	-0.246±0.079	0.786±0.017	0.779±0.016	3.041±0.043
2012.08.17	0.365±0.025(50)	0.270±0.041(57)	0.166±0.004(66)	+0.216±0.041	+0.002±0.051	0.890±0.054	0.879±0.015	3.453±0.034
2013.08.08	0.397±0.014(51)	0.240±0.014(72)	0.118±0.003(58)	-0.007±0.018	-0.041±0.015	0.481±0.021	0.538±0.005	2.893±0.020
2013.08.09	0.347±0.016(99)	0.206±0.014(136)	0.098±0.005(124)	-0.066±0.018	-0.032±0.014	0.552±0.022	0.591±0.009	2.991±0.024
2013.08.10	0.439±0.025(79)	0.328±0.042(109)	0.149±0.006(116)	-0.126±0.024	-0.097±0.038	0.431±0.060	0.559±0.015	2.908±0.037
2014.08.27	0.585±0.080(41)	0.363±0.076(75)	0.273±0.010(80)	-0.017±0.149	+0.002±0.097	1.124±0.109	1.102±0.032	3.492±0.111
2014.09.24	0.330±0.071(86)	0.263±0.070(90)	0.130±0.010(102)	-0.038±0.136	-0.065±0.084	0.944±0.104	1.006±0.030	3.487±0.102
2016.08.07	0.585±0.097(74)	0.345±0.053(74)	0.176±0.026(73)	-0.357±0.110	-0.096±0.056	1.238±0.078	1.346±0.035	3.542±0.133
2016.08.08	0.411±0.066(69)	0.243±0.064(73)	0.147±0.020(72)	-0.132±0.073	-0.017±0.068	1.342±0.091	1.366±0.030	3.778±0.096
2016.09.28	0.311±0.059(95)	0.214±0.064(96)	0.106±0.024(96)	-0.025±0.107	-0.054±0.069	1.340±0.090	1.381±0.034	3.824±0.082
2016.10.08	0.308±0.061(80)	0.151±0.041(81)	0.104±0.018(89)	+0.091±0.110	-0.003±0.048	1.444±0.063	1.391±0.027	3.807±0.089
2018.07.17	0.578±0.128(34)	0.351±0.090(41)	0.140±0.041(49)	-0.139±0.146	-0.108±0.084	1.944±0.128	2.083±0.060	4.216±0.186
2018.08.13	0.403±0.164(27)	0.198±0.085(31)	0.172±0.048(30)	+0.072±0.176	+0.061±0.090	1.490±0.126	1.449±0.074	3.778±0.241
2018.08.14	0.266±0.121(61)	0.195±0.056(55)	0.103±0.023(54)	+0.266±0.121	-0.034±0.056	1.476±0.081	1.540±0.036	3.960±0.170
2018.10.06	0.580±0.062(44)	0.262±0.047(41)	0.148±0.019(44)	-0.075±0.079	-0.030±0.057	1.391±0.071	1.475±0.031	3.538±0.097
2018.11.05	0.502±0.078(43)	0.232±0.046(46)	0.128±0.020(51)	-0.117±0.095	-0.037±0.050	1.488±0.070	1.550±0.031	3.724±0.121
2018.11.06	0.521±0.062(44)	0.226±0.046(45)	0.124±0.018(54)	-0.122±0.069	-0.021±0.052	1.512±0.068	1.570±0.028	3.718±0.093
2019.07.30	0.498±0.092(45)	0.293±0.079(50)	0.208±0.026(49)	-0.068±0.108	+0.026±0.082	1.799±0.116	1.782±0.037	4.162±0.116
2019.09.29	0.471±0.074(57)	0.298±0.061(72)	0.175±0.021(73)	+0.101±0.114	-0.004±0.072	1.783±0.091	1.834±0.032	4.176±0.110
2019.09.30	0.413±0.069(66)	0.285±0.061(78)	0.182±0.022(84)	+0.014±0.094	+0.029±0.069	1.850±0.092	1.853±0.033	4.338±0.102
2020.07.21	0.533±0.124(53)	0.307±0.052(52)	0.119±0.018(47)	-0.322±0.098	-0.106±0.040	2.089±0.079	2.202±0.025	4.421±0.182
2020.07.22	0.465±0.130(43)	0.431±0.081(45)	0.157±0.032(52)	-0.221±0.133	-0.237±0.085	1.904±0.124	2.151±0.048	4.470±0.191
2020.07.23	0.493±0.116(42)	0.272±0.058(45)	0.135±0.022(52)	-0.272±0.107	-0.097±0.050	2.130±0.088	2.174±0.033	4.491±0.169
2021.07.06	0.469±0.155(30)	0.273±0.085(30)	0.193±0.035(39)	-0.200±0.117	+0.003±0.070	2.754±0.111	2.640±0.044	5.178±0.198
2021.07.07	0.370±0.083(50)	0.319±0.064(56)	0.230±0.025(58)	-0.093±0.086	+0.053±0.063	2.733±0.111	2.624±0.033	5.318±0.108
2021.10.08	0.393±0.027(65)	0.218±0.018(82)	0.154±0.007(78)	+0.055±0.046	+0.009±0.063	2.796±0.029	2.673±0.012	5.216±0.042
2021.10.09	0.399±0.029(67)	0.244±0.020(76)	0.139±0.007(74)	-0.005±0.047	-0.004±0.022	2.757±0.031	2.699±0.012	5.195±0.044
2021.10.11	0.607±0.056(58)	0.395±0.064(70)	0.211±0.019(65)	+0.414±0.072	-0.080±0.083	2.684±0.079	2.710±0.025	5.090±0.071
2022.06.23	0.712±0.069(33)	0.560±0.093(34)	0.305±0.026(35)	-0.472±0.128	-0.204±0.124	2.948±0.123	3.014±0.032	5.428±0.092
2022.08.04	0.566±0.154(72)	0.354±0.048(67)	0.231±0.016(60)	+0.326±0.165	-0.058±0.051	3.123±0.064	3.018±0.023	5.500±0.709
2022.08.31	0.470±0.067(71)	0.263±0.045(70)	0.182±0.014(65)	-0.005±0.056	-0.025±0.044	0.558±0.058	0.605±0.019	2.916±0.084
2022.09.01	0.641±0.123(72)	0.486±0.124(74)	0.173±0.014(67)	-0.153±0.164	-0.263±0.151	0.342±0.160	0.622±0.018	2.757±0.159
2022.09.21	0.553±0.060(81)	0.330±0.045(85)	0.177±0.015(92)	-0.078±0.071	-0.050±0.048	0.561±0.058	0.658±0.020	2.924±0.020
2022.09.22	0.536±0.092(70)	0.318±0.052(79)	0.133±0.018(90)	-0.354±0.136	-0.125±0.061	0.579±0.068	0.710±0.023	2.942±0.116
2022.10.26	0.454±0.048(95)	0.343±0.039(102)	0.157±0.015(113)	-0.224±0.061	-0.110±0.038	0.576±0.048	0.718±0.018	3.035±0.059
2022.10.27	0.410±0.044(97)	0.255±0.030(99)	0.167±0.014(104)	-0.068±0.059	+0.005±0.034	0.670±0.040	0.695±0.018	3.101±0.057
2022.12.21	0.482±0.025(86)	0.235±0.024(79)	0.170±0.008(84)	-0.087±0.038	+0.002±0.028	0.780±0.033	0.729±0.013	3.121±0.036
2023.01.19	0.383±0.037(87)	0.275±0.039(85)	0.128±0.010(83)	-0.024±0.045	-0.068±0.043	0.729±0.050	0.779±0.013	3.266±0.048
2023.08.16	0.468±0.054(99)	0.413±0.043(95)	0.270±0.019(97)	+0.087±0.064	-0.100±0.050	0.853±0.054	0.950±0.023	3.442±0.067
2023.08.22	0.474±0.057(103)	0.312±0.046(111)	0.214±0.020(115)	+0.015±0.073	+0.019±0.050	0.970±0.056	0.970±0.024	3.414±0.070
2024.04.28	0.545±0.062(83)	0.445±0.069(84)	0.230±0.021(87)	-0.175±0.092	-0.156±0.082	1.049±0.088	1.187±0.027	3.582±0.076
2024.06.10	0.530±0.051(73)	0.334±0.054(80)	0.205±0.016(81)	-0.133±0.080	-0.024±0.060	1.218±0.072	1.263±0.022	3.608±0.065
2024.06.11	0.503±0.058(67)	0.418±0.062(64)	0.277±0.018(72)	+0.028±0.075	-0.025±0.067	1.178±0.082	1.232±0.024	3.707±0.073
2024.07.09	0.481±0.061(52)	0.290±0.060(68)	0.208±0.021(72)	-0.177±0.152	+0.026±0.078	1.409±0.082	1.351±0.028	3.867±0.078
2024.08.01	0.561±0.059(76)	0.385±0.063(74)	0.204±0.020(77)	-0.006±0.073	-0.081±0.064	1.310±0.077	1.368±0.025	3.767±0.076
2024.08.09	0.515±0.046(74)	0.330±0.049(80)	0.195±0.015(79)	+0.073±0.061	-0.034±0.052	1.428±0.064	1.407±0.021	3.897±0.062
2024.09.29	0.522±0.038(100)	0.279±0.043(99)	0.177±0.016(102)	+0.061±0.055	-0.017±0.052	0.926±0.055	0.976±0.023	3.236±0.050
Median	0.481 ± 0.097	0.303 ± 0.086	0.174 ± 0.050	-0.048 ± 0.164	-0.034 ± 0.072	1.274 ± 0.751	1.384 ± 0.713	3.658 ± 0.755

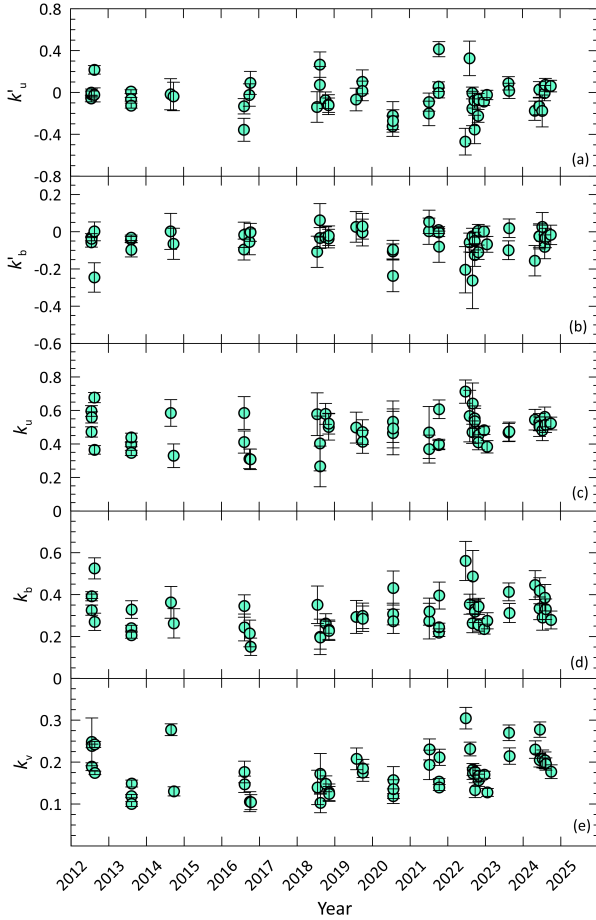


Figure 3. Variation of the primary and secondary extinction coefficients from 2012 to 2024.

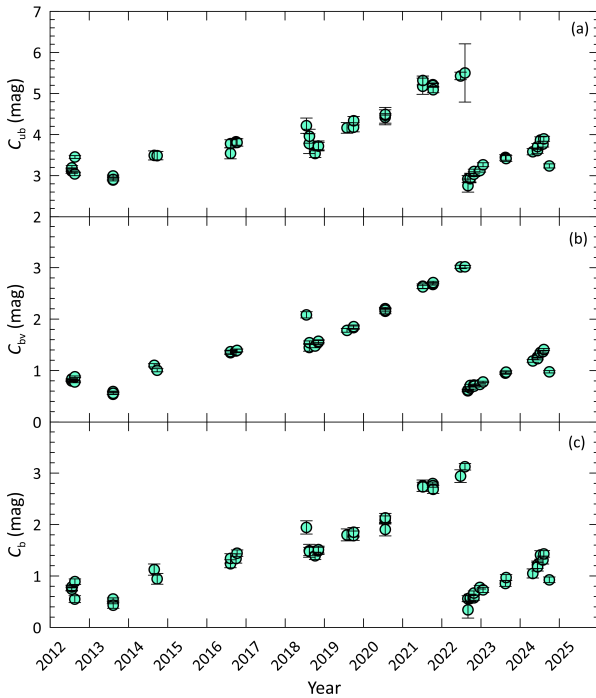


Figure 4. Variation of zero points from 2012 to 2024.

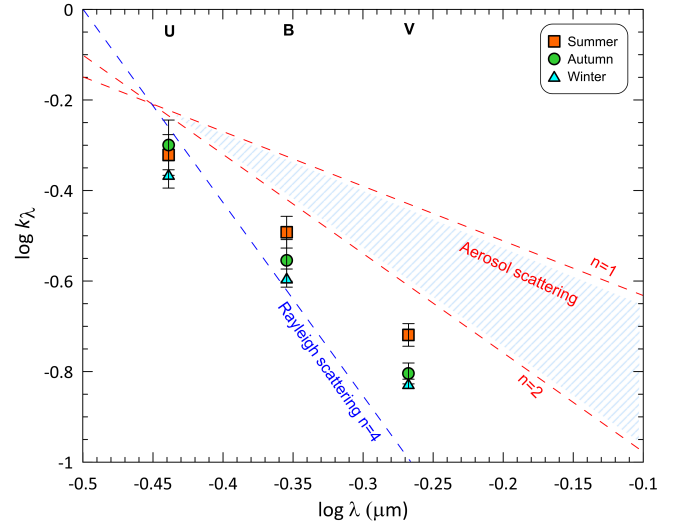


Figure 5. Variation of seasonal median values of extinction coefficients with wavelength. The shaded part represents the area affected by scattering due to aerosols and dust, while the line with $n=4$ represents the pure Rayleigh scattering.

When extinction is caused by aerosol and dust, then n is between 1 and 2. Seasonal averages are shown in Figure 5, where extinction coefficient variation with wavelength are also drawn for $n=1$, $n=2$, and $n=4$. Figure 5 shows that extinction during winter and autumn is almost entirely due to Rayleigh scattering. For the summer season, the source of extinction is mainly Rayleigh scattering although aerosol scattering has some effect.

3.4. Comparison with Landolt's catalogue

In order to find differences between the T100 and Landolt's photometric systems, we estimated differences of standard star' V magnitudes and $U - B$ and $B - V$ colour indices calculated from our transformation equations and the ones taken from Landolt's catalogues (Landolt 2009, 2013) for 34 nights between 2018 and 2024. Since there are 2188, 2421, and 2324 standard star observations for $U - B$, $B - V$, and V in these nights, respectively, we calculated median values of the differences for 0.1 mag intervals of $U - B$ and $B - V$ colour indices. The distribution of the median values with respect to the corresponding color indices is shown in Figure 6. Here Δ indicates the calculated value minus the catalogue value. Means and standard deviations of $\Delta(U - B)$, $\Delta(B - V)$, and ΔV were estimated to be 1.4 ± 76 , 1.9 ± 18 , and 0.0 ± 36 mmag, respectively.

Figure 6 reveals that there are systematic differences between the T100's and Landolt's photometric systems for the U -band. Differences between the two systems in $U - B$ follow a sinusoidal-like curve against $U - B$ and $B - V$. However, the median differences are relatively small ($|\Delta(U - B)| \leq 0.05$) for stars with $-0.5 < U - B$ (mag) < 1.6 and $0.2 < B - V$ (mag) < 1.8 , although it is considerably high for bluer and redder stars. This difference probably originates from the quantum efficiency

Table 3. The transformation coefficients calculated for each observing night. Median values are given in the last line, where errors are standard deviations of the individual values.

Date	α_b	α_{bv}	α_{ub}
2012.07.18	0.930±0.043	0.056±0.006	0.926±0.054
2012.07.19	0.992±0.038	0.077±0.011	0.861±0.050
2012.07.20	0.936±0.018	0.051±0.003	0.813±0.056
2012.08.16	1.253±0.105	0.084±0.011	0.836±0.093
2012.08.17	0.919±0.066	0.081±0.011	0.537±0.055
2013.08.08	0.972±0.024	0.070±0.003	0.840±0.027
2013.08.09	0.959±0.023	0.068±0.006	0.951±0.028
2013.08.10	1.045±0.055	0.069±0.010	1.038±0.037
2014.08.27	0.869±0.137	0.041±0.022	0.853±0.221
2014.09.24	1.004±0.124	0.086±0.020	0.929±0.196
2016.08.07	1.031±0.086	0.057±0.009	1.378±0.166
2016.08.08	0.920±0.095	0.056±0.007	0.613±0.105
2016.09.28	0.968±0.099	0.058±0.010	0.849±0.146
2016.10.08	0.900±0.073	0.068±0.008	0.754±0.158
2018.07.17	1.046±0.122	0.049±0.014	1.023±0.218
2018.08.13	0.805±0.135	0.045±0.017	0.730±0.266
2018.08.14	0.967±0.079	0.072±0.008	0.444±0.172
2018.10.06	0.978±0.084	0.101±0.011	0.988±0.120
2018.11.05	0.968±0.076	0.078±0.008	0.977±0.142
2018.11.06	0.932±0.077	0.073±0.007	0.986±0.102
2019.07.30	0.866±0.127	0.073±0.011	0.953±0.161
2019.09.29	0.900±0.107	0.062±0.008	0.684±0.166
2019.09.30	0.852±0.105	0.066±0.008	0.801±0.137
2020.07.21	1.057±0.064	0.071±0.009	1.304±0.157
2020.07.22	1.245±0.132	0.073±0.014	1.203±0.203
2020.07.23	1.044±0.081	0.066±0.010	1.221±0.161
2021.07.06	0.874±0.099	0.060±0.014	1.043±0.163
2021.07.07	0.810±0.090	0.063±0.013	0.882±0.115
2021.10.08	0.893±0.030	0.088±0.007	0.776±0.066
2021.10.09	0.920±0.035	0.078±0.006	0.891±0.071
2021.10.11	0.988±0.101	0.053±0.010	0.282±0.094
2022.06.23	1.165±0.163	0.082±0.013	1.426±0.166
2022.08.04	0.961±0.070	0.074±0.010	0.565±0.900
2022.08.31	0.956±0.059	0.065±0.008	0.842±0.074
2022.09.01	1.222±0.194	0.084±0.008	0.999±0.213
2022.09.21	0.968±0.063	0.074±0.008	0.945±0.096
2022.09.22	1.092±0.084	0.091±0.010	1.422±0.179
2022.10.26	1.049±0.049	0.071±0.007	1.169±0.084
2022.10.27	0.920±0.046	0.081±0.008	0.972±0.085
2022.12.21	0.888±0.039	0.079±0.008	1.010±0.058
2023.01.19	0.958±0.058	0.065±0.008	0.855±0.064
2023.08.16	1.054±0.067	0.050±0.023	0.715±0.082
2023.08.22	0.890±0.064	0.076±0.009	0.840±0.093
2024.04.28	1.075±0.106	0.046±0.013	1.038±0.116
2024.06.10	0.928±0.082	0.060±0.012	1.027±0.106
2024.06.11	0.926±0.093	0.067±0.012	0.797±0.096
2024.07.09	0.861±0.112	0.071±0.012	0.956±0.175
2024.08.01	1.001±0.081	0.071±0.010	0.835±0.094
2024.08.09	0.947±0.069	0.082±0.010	0.681±0.083
2024.09.29	0.926±0.068	0.062±0.011	0.738±0.073
Median	0.958 ± 0.100	0.070 ± 0.013	0.886 ± 0.228

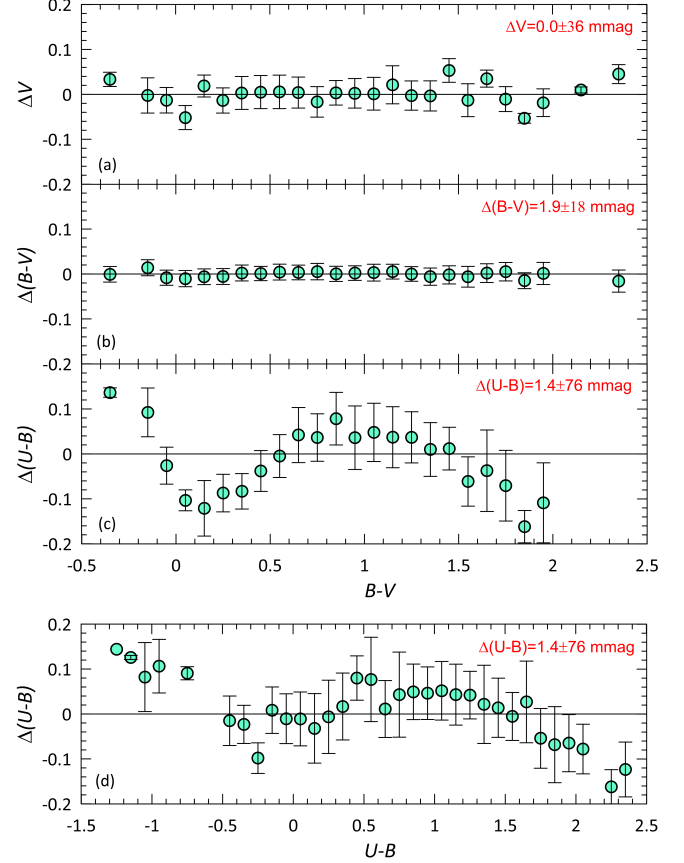


Figure 6. Median $\Delta(U - B)$, $\Delta(B - V)$, and ΔV values against colour indices. Δ means calculated minus catalogue (Landolt 2009, 2013) value. Median values were calculated for 0.1 mag intervals of related colour index. Means and standard deviations of $\Delta(U - B)$, $\Delta(B - V)$, and ΔV are given in panels.

of detectors used in the two photometric systems. As for the differences of $\Delta(B - V)$ and ΔV , Figure 6 shows that transformation equations found for the T100 photometric system work well. The median values of $|\Delta(B - V)|$ are smaller than 15 mmag for stars with $-0.4 < B - V$ (mag) < 2.4 , while almost all median values of $|\Delta V|$ are smaller than 20 mmag for stars with $-0.2 < B - V$ (mag) < 1.8 . Thus, we conclude that the T100's photometric system well matches that of Landolt's photometric systems for $B - V$ and V .

4. SUMMARY

We observed many standard stars selected from Landolt (2009, 2013) with the Bessell UBV filters during 50 nights from the year 2012 to 2024 with the 1-meter telescope (T100) of the TÜBİTAK National Observatory to perform photometric analysis of open clusters. As a byproduct, we derived precise transformation relations for the T100 photometric system.

1. Primary and secondary atmospheric extinction coefficients were determined for nights with photometric conditions. Median values of primary extinction coefficients were found to

be 0.481 ± 0.097 , 0.303 ± 0.086 , and 0.174 ± 0.050 for U , B , and V filters, respectively. Median secondary extinction coefficients k'_u and k'_b were calculated as -0.048 ± 0.164 and -0.034 ± 0.072 , respectively. We found that primary extinction coefficients do not show a strong seasonal variation. We conclude that the median values of extinction coefficients estimated for summer and autumn are very similar within errors. Seasonal values of the coefficients and number of usable nights show that the winter and spring can not be favourite seasons for photometric observations at the TÜBİTAK National Observatory.

2. Our observations span a 12-year period from 2012 to 2024, excluding the years 2015 and 2017, allowing us to determine the variation in extinction coefficients over this time. We found that primary extinction coefficients decreased from the year 2012 to 2019, while they increased from 2019 to 2024, indicating deterioration of photometric conditions starting from the year 2019. No systematic variation in the secondary extinction coefficients could be identified.

3. The values of photometric zero points for B , $B - V$, and $U - B$ gradually become fainter during years, as expected. In addition, we found a “jump” of zero points to brighter magnitudes in August 2022, corresponding to the cleaning of the main mirror of the telescope.

4. We investigated the characteristics of atmospheric extinction based on scattering mechanisms. It is found that Rayleigh scattering is the main reason for atmospheric extinction in autumn and winter seasons, while aerosol scattering has some effect on the extinction in summer.

5. It is found that there are systematic differences for the U -band between the T100' and Landolt's photometric systems, although the median differences are relatively small for stars with $-0.5 < U - B$ (mag) < 1.6 and $0.2 < B - V$ (mag) < 1.8 . This difference probably originates from the quantum efficiency of detectors used in the two photometric systems. We conclude that transformation equations found for the T100' photometric system work well for V and $B - V$ as the median values of $|\Delta(B - V)|$ and $|\Delta V|$ are small for a wide range of $B - V$ colour index. As a result, we also conclude that the T100's photometric system acceptably well matches that of Landolt's photometric systems for $U - B$, $B - V$, and V .

6. As a general result, we finally conclude that the transformation relations found in this study can be used for standardized photometry with T100's photometric system.

Peer Review: Externally peer-reviewed.

Author Contribution: Conception/Design of study - T.A., R.C., T.Y.; Data Acquisition - T.A., R.C., T.Y.; Data Analysis/Interpretation - T.A., R.C., T.Y.; Drafting Manuscript - T.A., R.C., T.Y.; Critical Revision of Manuscript - T.A., R.C., T.Y.; Final Approval and Accountability - T.A., R.C., T.Y.

Conflict of Interest: Authors declared no conflict of interest.

Financial Disclosure: This study has been supported in part by the Scientific and Technological Research Council (TÜBİTAK) 113F270.

Acknowledgements: We thank to TÜBİTAK National Observatory for partial support in using the T100 telescope with project numbers 15AT100-738 and 18CT100-1396. We also thank to the on-duty observers and members of the technical staff at the TÜBİTAK National Observatory for their support before and during the observations.

LIST OF AUTHOR ORCIDS

T. Ak <https://orcid.org/0000-0002-0688-1983>
 R. Canbay <https://orcid.org/0000-0003-2575-9892>
 T. Yontan <https://orcid.org/0000-0002-5657-6194>

REFERENCES

- Golay M., 1974, Introduction to astronomical photometry, doi:10.1007/978-94-010-2169-2.
- Janes K., Barnes S. A., Meibom S., Hoq S., 2013, *AJ*, **145**, 7
- Johnson H. L., Morgan W. W., 1953, *ApJ*, **117**, 313
- Kilkenny D., van Wyk F., Roberts G., Marang F., Cooper D., 1998, *MNRAS*, **294**, 93
- Landolt A. U., 2009, *AJ*, **137**, 4186
- Landolt A. U., 2013, *AJ*, **146**, 131
- Menzies J. W., Cousins A. W. J., Banfield R. M., Laing J. D., 1989, South African Astronomical Observatory Circular, **13**, 1
- Menzies J. W., Marang F., Laing J. D., Coulson I. M., Engelbrecht C. A., 1991, *MNRAS*, **248**, 642
- Sung H., Bessell M. S., 2000, *Publ. Astron. Soc. Australia*, **17**, 244